Chapter 1
Domain Boundary Engineering in Ferroic and Multiferroic Materials: A Simple Introduction

Ekhard K.H. Salje and Jason C. Lashley

Abstract Multiferroic behavior is commonly described as a bulk phenomenon where, at least, two of the three ferroic properties, ferromagnetism, ferroelectricity, and ferroelasticity, coincide. This notion is enlarged to contain as another "useful" property electrical conductivity. While bulk applications are potentially useful, we describe the recent development where the same properties are restricted to domain boundaries or interfaces, while the adjacent domains are not active elements themselves. This means that the information is restricted to thin, nearly two-dimensional slabs of some 2 nm thickness. The information density is, thus, extremely high, while conducting interfaces can serve as wires to connect the active elements. In this chapter, we discuss the underlying physical principles for the "engineering" of interfacial multiferroics.

1.1 Introduction

Multiferroicity combines at least two of the three ferroic properties of a material: ferroelasticity, ferroelectricity, or ferromagnetism. Its investigation has a long tradition with significant work on boracites in the 1960s [1] and a continuous stream of activities on ceramics with perovskite-like structures [2–8]. In addition, it was realized that "ferroelastics" and "martensites" describe the same materials properties that have simply different historic traditions for their naming (so that "ferroelastic" alloys are usually called "martensites" and have often, but not

E.K.H. Salje (✉)
University of Cambridge, Downing Street, Cambridge CB 2 3EQ, Cambridge, UK
e-mail: es10002@esc.cam.ac.uk

J.C. Lashley
Los Alamos National Laboratory, Los Alamos, NM, USA
e-mail: j.lash@lanl.gov

T. Kakeshita et al. (eds.), *Disorder and Strain-Induced Complexity in Functional Materials*, Springer Series in Materials Science 148,
DOI 10.1007/978-3-642-20943-7_1, © Springer-Verlag Berlin Heidelberg 2012

always, step-wise phase transitions [9], while ceramics and minerals, which have "martensitic" properties, are usually called "ferroelastics"). Magnetic martensites, for example, are multiferroics and follow the same physical mechanism as the very large number of ferromagnetic *cum* ferroelastic ceramics.

The motivation for the investigation of multiferroic materials is that better memory devices can be made from such compounds [10, 11]. For this purpose, ferroelasticity is of minor importance because reading/writing mechanisms will rely on magnetic or electric fields so that the key for the development of multiferroics is the combination of ferroelectric and ferromagnetic properties. The role of ferroelasticity is nevertheless often a key for the performance of such devices: coupling between different ferroic properties can be "strain-induced" where both properties couple strongly with some lattice distortion (via magnetostriction and electrostriction or piezoelectricity, etc.) and, thus, couple with each other. Strain-induced coupling occurs on an atomic scale [12, 13] or on a mesoscopic scale [14–16], whereby the latter allows further development of enhanced strains via microengineering resolution patterning and processes.

Current work on structural multiferroics was revived with work focussing mainly on $BiFeO_3$ [17–20]. Two further developments have occurred after 2000, which may lead to even more effective multiferroic device materials. Firstly, coupling with charge carriers is now subject to much research. Here, the combination between a magnetically or electrically written signal and its reading via high conductivity regions in a material has become an attractive proposition [21–25]. Such regions can be grain boundaries, interfaces, or twin boundaries or be part of exsolution patterns or amorphized/glassy clusters [26–28]. The second development leads this idea even further: why not to take such interfacial regions as active elements of the multiferroic properties themselves. This restricts the size of the active element to a few nm in thickness, while the crystal simply serves as matrix in which such heterostructures are located. It is the purpose of this introduction to highlight some of the developments that lead to the emerging field of "domain boundary engineering" which, potentially, brings the size of active elements, say in memory devices, from currently 0.1 μm to well below 50 nm and also allows a truly 3D arrangement of multiferroic elements.

1.2 Multiferroic Domain Boundaries

Domain boundaries, in particular twin boundaries, which are discussed now, show reduced chemical bonding with many of the structural constituents. With respect to elastic, magnetic, or electric susceptibilities, one expects domain boundaries to be "softer" than the bulk, although such softening can hardly be measured macroscopically because the volume proportion of interfaces is relatively small compared with the bulk. An exception is – in some measure – relaxor materials where the relaxor regions themselves have wall properties (for order–disorder systems) and show indeed strong finite size effects and soft susceptibilities [29–31].

Nevertheless, twin boundaries can reach several parts-per-million of the sample volume so that large signals from internal ferroic properties of the boundaries may even compete with the macroscopic properties of the bulk. The advantage of the localized wall properties is their high information density: they are contained within very thin sheets of twin walls and can be addressed spatially with very high resolution. This means that the storage density of information encrypted in twin walls is extremely high so that wall-related devices could theoretically outperform bulk devices by several orders of magnitude.

The second ingredient is the condition that structural gradients of twin walls extend over several interatomic distances. In Fig. 1.1, a high resolution electron microscopy image of a twin wall in $NdGaO_3$ is shown where the imaging condition was optimized for atoms inside the twin wall, while atoms outside the wall are slightly out of imaging condition by inclination of their lattice plane from the plane of diffraction. The "thickness" of the twin wall can now be estimated by simply counting the number of unit cells in the wall. The resulting wall thickness of ca. 2 nm compares well with results from diffraction experiments at low temperatures in interfaces and surfaces [32–34]. The wall thickness increases when the transition point is approached. Careful analysis of the diffuse diffraction of wall-related signals in $LaAlO_3$ showed that the wall thickness increases according to the predictions of Landau–Ginzburg theory for a second-order phase transition [8, 33]. In first-order martensitic transitions, the effect is smaller although the increase follows still the scaling of the correlation length of the phase transition, which leads to significant increases near the transformation point in compounds such as NiTi and NiTiFe [35, 36].

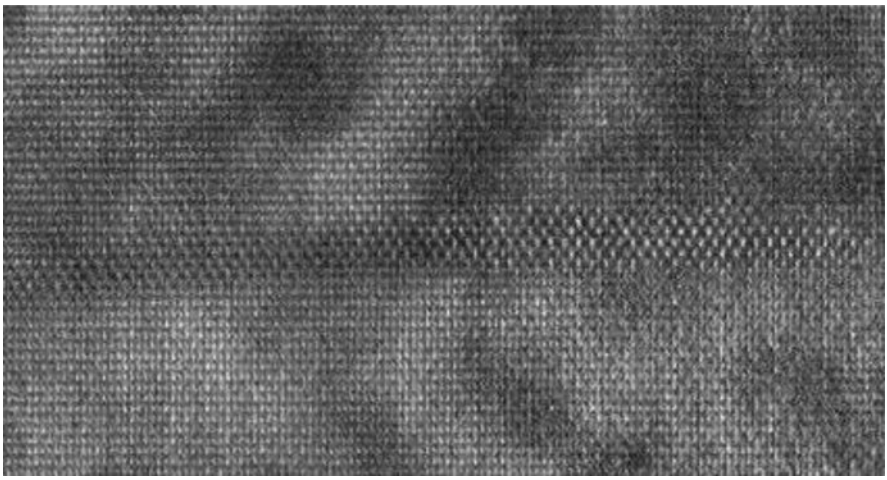

Fig. 1.1 Transmission electron microscopy image of NdGaO3 (Pbnm) near a {101} twin boundary in the middle of the figure. The unit cell is $a = 0.5426$ nm, $b = 0.5502$ nm, and $c = 0.7706$ nm for the orthorhombic cell and $a = b = 0.3864$ nm and $c = 0.3853$ nm for a perovskite-related cell. The thickness of the interface is 2w $\sim$ 6 unit layers or $\sim$2.3 nm (photograph courtesy G. Van Tendeloo, Antwerp)

The discovery of ferroic properties of interfaces is often related to computer simulations for materials design and the theoretical exploration of extreme physical properties in solids. Such research expands from inorganic materials to biological samples in life sciences. We first discuss an example in solid state physics where sizeable spontaneous polarization was predicted in {100} twin walls of $CaTiO_3$, a definitely nonpolar material [37, 38]. Theoretical simulations [39–41] of these walls show an extremely rich texture of the local polarization at and close to the walls. Local distortions include a strong antiferroelectric component, and local nonzero contributions perpendicular to the wall plane, which do not contribute to the macroscopic net dipole moment. Individual Ti displacements of 2 pm off the octahedron center give rise to a net polarization corresponding to a displacement of 0.6 pm in the direction of the bisector of the twin angle. The effect is intrinsically coupled with the appearance of twin boundaries in the matrix, which was already previously identified as locality of oxygen vacancies in $CaTiO_3$ [37, 41].

While indirect evidence for the polar behavior of twin walls has been reported before [42], as well as in antiphase boundaries, APBs [43], and grain boundaries [44], the results in $CaTiO_3$ are very instructive as it was the first clear indication of twin wall polarity and the underlying structural mechanism for the coupling between strain and dipole moments. $CaTiO_3$ is orthorhombic in its low-temperature form (space group Pnma) and is purely ferroelastic. No ferroelectric features have ever been recorded. The TiO_6 octahedron, on the other hand, is well known for its tendency to form polar groups where the Ti position is offcentered with respect to the geometrical center of the surrounding oxygen atoms. Such polar structures exist in compounds such as $BaTiO_3$, $PbTiO_3$, and others. The known competition with octahedral rotation [45] in the tetragonal and orthorhombic phases of $CaTiO_3$ suppresses the off-centering. It is, however, restored when the rotation angle vanishes or when the density of the material decreases. Both conditions are met inside the twin wall and it is thus not entirely unexpected that twin walls should show dipolar moments. What was unknown is the actual size of the polarization and the texture of the polarization field.

To investigate polar ordering in the ferroelastic walls of $CaTiO_3$, numerical simulations were performed based on an atomic-scale description of the walls in which atoms interact via empirically defined forces [37–42]. Periodic boundary conditions were used in three dimensions. Open boundary conditions in the direction perpendicular to the walls would imply surfaces, which would add unwanted complexity to the problem. Two twin walls are needed to conform to periodic boundary conditions. A supercell was built of 26 unit cells in the direction x perpendicular to the walls, six unit cells in the direction perpendicular to the plane of the twin angle (z), and ten unit cells in the bisector of the twin angle y (using the unit cell of the prototypic cubic structure). This gives a total of 7,800 atoms. Figure 1.2 shows the primary order parameter Q as a function of x, in the direction perpendicular to the wall. Q is a measure of the rotation around the y axis of the oxygen octahedra around each titanium atom, appropriately sign corrected. The dashed line indicates the fitted $Q \sim \tan h(x/w)$ functional form which is expected from Landau theory [8]. The wall width lies well within the experimental values

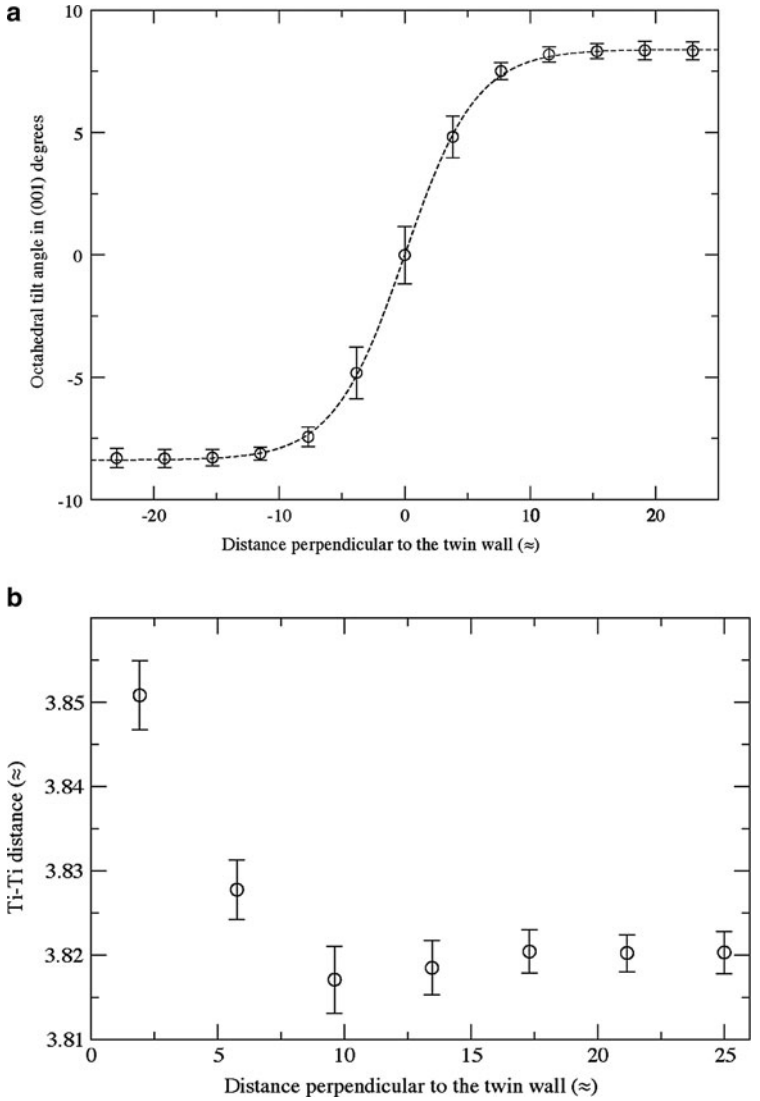

Fig. 1.2 (**a**), (**b**) Profile of the twin wall in $CaTiO_3$. The primary order parameter is the rotation of the TiO_6 octahedra. The twin boundary shows an inversion of the rotation angle (Fig. 1.1a) where the *dotted line* indicates the predictions from Landau–Ginzburg theory. The secondary order parameter is the widening of the unit cell, which is measured by the distance between two adjacent Ti positions. Figure 1.1b shows the increase of the Ti–Ti distance in the wall by ca. 1%, which is sufficient to induce off-centering of the Ti atom from the middle of the octahedra and also an increase of the mobility of defects

as determined previously [33]. The secondary order parameter of interest here is the off-centering of Ti from the center of charge of the corresponding oxygen octahedron. The largest displacements are of 2.0 pm, mostly along the z direction.

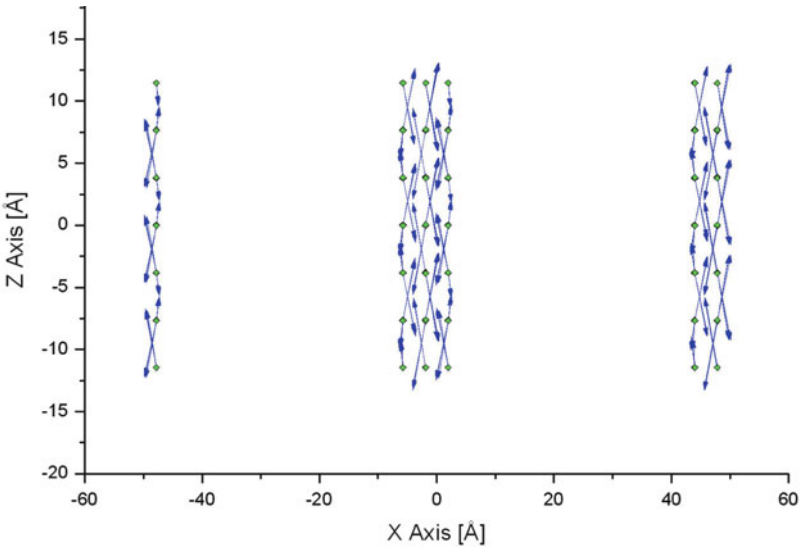

Fig. 1.3 Patterns of the off-centering of Ti from the midpoint of the oxygen octahedra in $CaTiO_3$. The graph shows the displacement patterns in the direction to the twin walls

Two types of off-centering are seen (Fig. 1.3) within the domain wall. The largest component is the one along the z direction antiferroelectric with alternating Ti positions shifted in opposite directions. In contrast, the off-centering along the y direction is ferroelectric and produces a net dipole moment for each domain wall equivalent to a net displacement of 0.6 pm per Ti atom (0.9 pm for the second force field). There is also a smaller antiferroelectric component along the direction perpendicular to the wall, x.

In addition to the appearance of polar properties of the walls, an increase of oxygen vacancies was also predicted. An oxygen vacancy gains ca. 1.1 eV when shifted from the bulk of the material into the twin wall [41]. While this effect is expected from the fact that twin walls in the geological context are known to be decorated by defects, we understand from these calculations that the geometrical requirement for the accommodation of defects may appear negligible, namely, ca.1% increase of a lattice spacing in $CaTiO_3$. Such small changes are typical for twin boundaries and other interfaces so that the observation that dopants are concentrated in interfaces is not unexpected. These localized dopants, on the other hand, can then be used systematically to modify the properties of the walls, e.g., their conductivity or polarity. Doping with magnetic ions may then lead to magnetic properties of the walls, while the same dopants would not necessarily enter the bulk.

The widening of the unit cell at the interface could also lead to a reduction of the local elastic response. This does not mean that the position of a twin wall can be shifted by external forces (which it can), but the compressibility of the wall itself is larger than the equivalent compressibility of the bulk. While such an effect has been seen [40], it appears that the effect is much smaller than could be expected

by the simple reduction of the density in the wall. In fact, the reduction of the relevant elastic modulus as expected by the increase of the distance between nearest neighbous is partly compensated by the decrease of the distance of the next nearest neighbous [46] so that the relaxation of the structure compensates to a large extent the elastic softening due to the swelling of the interface.

1.3 Highly Conducting Interfaces

We have argued that twin walls can attract defects, which leads to the possibility to dope twin boundaries selectively, i.e. to introduce defects into the boundaries but not in the bulk. This possibility was first used to change the conductivity in WO_3 in 1998 [21] with the introduction of Na and oxygen vacancies in twin walls [47–49]. The chemical composition of the walls was very slightly modified (e.g. from WO_3 to $WO_{2.95}$), which induced a metal–insulator transition and, at low temperature, led to the appearance of superconductivity in twin walls. The fact that the dopants follow the trajectories of the twin walls means that nanopatterning of the superconducting structure is possible via the patterning of the twin boundaries and subsequent doping (Figs. 1.4 and 1.5).

Tungsten oxide, WO_3, and its substoichiometric derivatives, WO_{3-x}, are particularly well suited for this research because they display metal–insulator transitions, while they remain thermodynamically stable compounds. They display a multitude of structural phase transitions [50] mainly related to shape changes of the WO_6 octahedra and their rotations within an octahedral network. WO_3 easily releases oxygen and incorporates alkali ions and hydrogen. The facility with which oxygen is released under reducing conditions is less related to the chemical bonding of

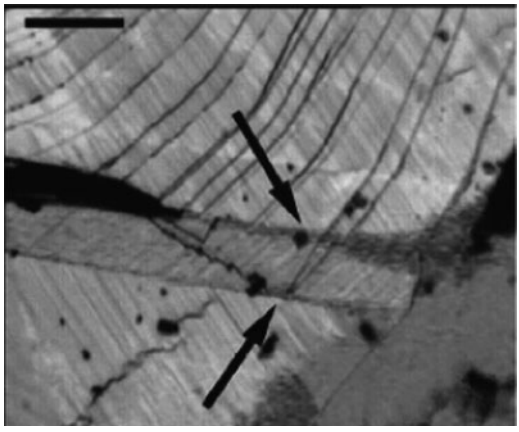

Fig. 1.4 superconducting twin walls (*arrows*) in WO_3 close to the crystal surface. The scale bar in the *top left corner* is 50 μm

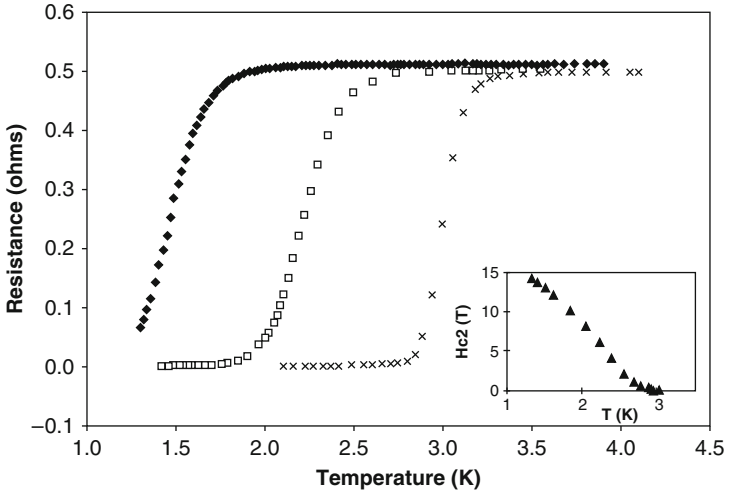

Fig. 1.5 Resistance of the superconducting twin wall in WO_3. The onset of superconductivity is 3 K; the critical field H_{c2} increases to 15 T at low temperatures

oxygen but rather to the low energy required to transfer the valence state of localized surplus electrons on the W^{6+} sites to W^{5+}. This tendency to form W^{5+} states near surfaces was directly confirmed by XPS/UPS experiments [51] and indirectly by STM imaging [52]. These W^{5+} states are not localized, however, and form bi-polarons in the low-temperature phase [53, 54]. WO_3 is a well-known electrochromic, solar cell, and catalytic material; it also displays the remarkable superconducting properties discussed before. Superconducting twin walls in WO_3 are chemically slightly reduced by inserting Na or removing O from the walls. The chemically modified walls (the changes are minor and analytically hard to detect) are then superconducting with a critical field H_{c2} above 15 T and a superconducting transition temperature T_C near 3 K. The surrounding matrix remains insulating so that this arrangement of superconducting twin boundaries with the formation of needle domains and domain junctions is potentially the key for engineering arrays of Josephson junctions and high sensitivity magnetic scanners. In addition, it has been suggested that surface layers, presumably similar to the interfacial structures in WO_3, may display superconductivity at temperatures up to $T_c = 91$ K (Na doping) and 120 K (H doping) [55]. These would constitute extreme values of T_c, which have not been reproduced independently, while the lower value in domain boundaries (3 K in [21]) has been directly observed by transport measurement and subsequently reproduced. In Fig. 1.6, we show the room temperature contrast as measured in AFM and PFM of a WO_3 surface. The highly conducting interfaces are clearly visible. The underlying bulk is piezoelectric, which ensures coupling with electric fields. In addition, it was reported that the ϵ-phase in WO_3 is ferroelectric [50] so that piezoelectric – ferroelectric – superconducting coupling becomes possible.

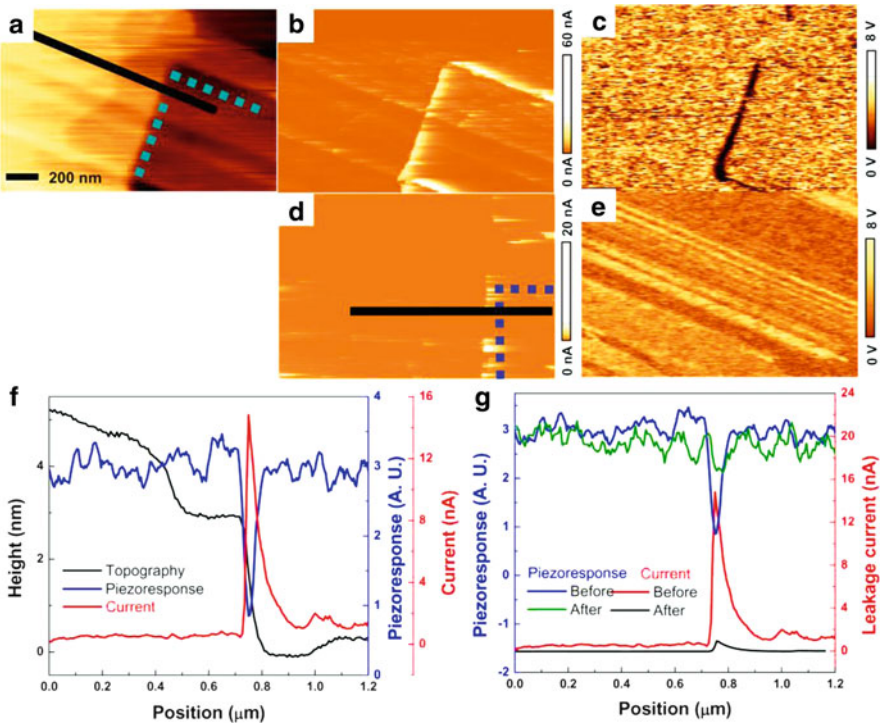

Fig. 1.6 (**a**) Topography, (**b**) current, and (**c**) PFM amplitude images of a freshly reduced WO_{3-x} single crystal. (**d**) Current and (**e**) PFM amplitude images of the same area of the WO_{3-x} single crystal as in (**a**) measured after several weeks. (**f**) Topography, current, and amplitude (piezoresponse) profiles acquired along the *black line* in (**a**), (**b**), and (**c**), respectively. (**g**) Current and amplitude (piezoresponse) profiles before and after an elapsed time of several weeks. The *dotted box* of (**a**) and (**d**) presents the steps to identify the location [56]

1.4 The Dynamics of Domain Movement and Ferroic Switching

If interfaces are taken to be the active elements of a material, the question arises whether such interfaces are stable under external forces or whether their location changes. This will decide their applicability: pinned interfaces will be used according to their internal dynamics, while mobile interfaces will change the size of the adjacent domains and, thus, operate similar classic ferroics where the size of the domains in the various orientations determines the response of a material with respect to external fields.

In multiferroics, the common view is that interfaces can move with external fields in a momentum-driven dynamics. The domains then propagate as classic front propagation [8] for large enough fields. For small field strength, this picture was shown to be wrong, however. Careful measurements under small thermal and elastic driving forces have revealed jerky front propagation and avalanche formation.

This phenomenon is well known in shape-memory alloys where the movement of interfaces between austenite and martensites leads to acoustic emission (AE) similar to Barkhausen-type avalanche behavior where – in the conventional picture – jerky propagation of one interface releases a multitude of other interfaces so that ultimately an avalanche of propagating phase fronts is observed [57]. Theoretically, such avalanches are expected to obey power law distributions [58] and can be considered to be at or near a point of selforganized criticality [59]. While this idea is appealing for its simplicity, it is hard to imagine that the randomness of the various pinning centers in martensites will not extend to extremely low values where pinning can occur only at very low temperatures. In fact, most experiments seem to indicate that pinning, depinning, and acoustic emission (AE) dynamics is a-thermal, which means that it is not thermally activated. A key experiment was recently performed [60] where the transition in a $Cu_{67.64}Zn_{16.71}Al_{15.65}$ shape-memory alloy was investigated calorimetrically, whereby the thermal driving force was minimized. The transition was scanned at rates of some mK/h so that each avalanche could be observed as an individual peak in the latent heat. The resulting DTA curve is shown in Fig. 1.7. It consists of two components: the jerks (Fig. 1.8) and a continuous background.

The entropy of the transition is not affected by the jerks and is the same on heating and cooling. Besides for the strongest avalanches, no memory effect was observed for the individual jerks. The statistical analysis of the jerks is the same as of AE spectra (Fig. 1.8) and follows a power law of the energy of the jerks: $P(E) \sim E^{-\varepsilon}$ with an exponent close to $-\varepsilon \sim -2$. This observation shows that the AE exponents are identical with or close to the energy exponents and not the size exponents (Fig. 1.9).

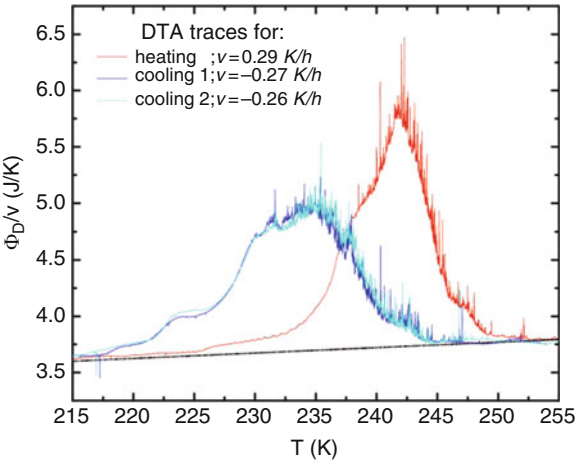

Fig. 1.7 DTA traces for cooling and heating experiments. The heating rate was 0.29 K/h, the cooling rates were 0.27 and 0.26 K/h. Note the coexistence of smooth front propagation and thermal spikes (jerks) even at very low thermal driving forces

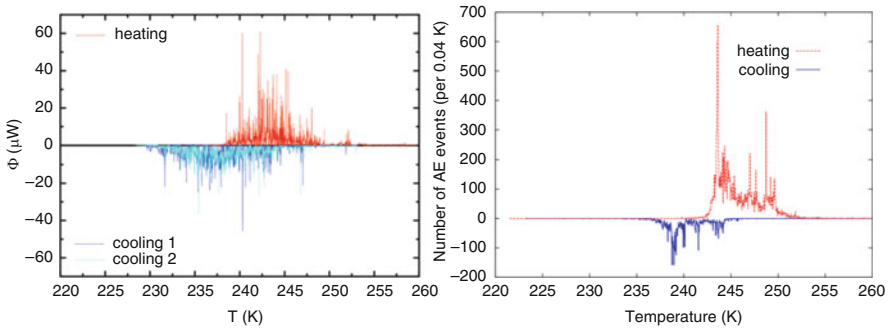

Fig. 1.8 Spikes in the calorimetric measurement after removing the smooth baseline (*left*) and acoustic emission (AE) signals (*right*) of the same sample. The sign of the peaks has been inverted for clarity between heating and cooling experiments [60]

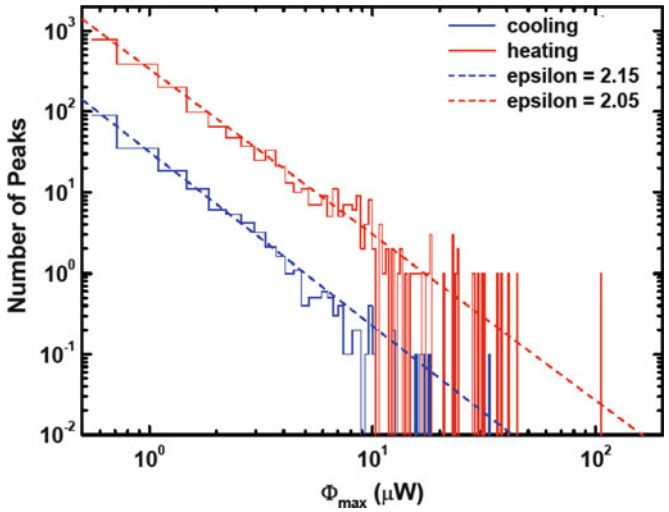

Fig. 1.9 Statistical analysis of the heating and cooling curves of the DTA traces in Fig. 1.3. Data corresponding to cooling experiments have been shifted one decade downward in order to clarify the picture [60]

A direct observation of the jerks in elastic measurements depends on the smallness of the applied forces. The transition in $Cu_{74.08}Al_{23.13}Be_{2.79}$ was investigated in a very careful dynamical mechanical analyzer (DMA) experiment. The frequency of the three-point-bending excitation was chosen as 0.1 Hz, the applied forces were extremely small (<50 mN max. amplitude), and the heating/cooling rate was <0.14 K/h. The mechanical loss is $\sim \tan(\delta)$ and shows spiky avalanche behavior (Fig. 1.10) similar to those in Fig. 1.8. Statistical analysis of the jerks leads again to a power law. The exponent (−1.3) is significantly smaller than the energy exponent of the calorimetric measurement, even though the uncertainty of the fitted exponent

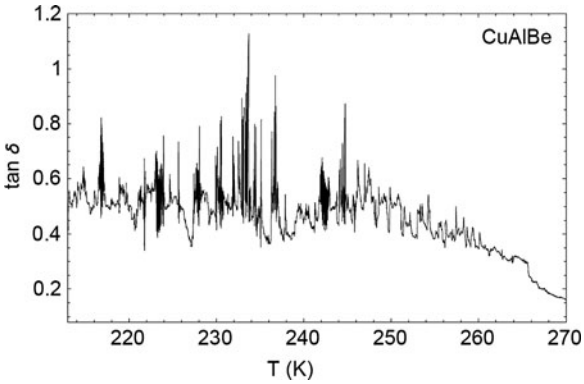

Fig. 1.10 Phase lag tan(δ) of a $Cu_{74.08}$ $Al_{23.13}$ $Be_{2.79}$ single crystal recorded in three-point-bending mode at 0.1 Hz and a heating rate of 0.15 K/h [61]

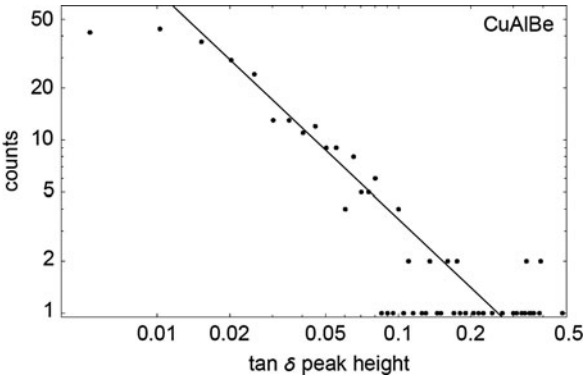

Fig. 1.11 Log–log plot of the peak statistics in Fig. 1.5. The *line* represents the best fit to a power law $P(E) \sim E^{-\varepsilon}$ with $\varepsilon = 1.3$ and an upper bound of 1.6 [61]

is very large. As an upper bound the exponent of -1.6 was estimated in [61]. As the elastic response is measured under oscillatory stress, one may expect that the exponent is related to field binning and related to the amplitude exponent $-\tau$, which was calculated to be in the order of -1.5 in MFT and near -1.3 in simulations [62] (Fig. 1.11).

The movement of interfaces between martensitic variants and ferroelastic twin walls depends theoretically on the dimension of the interface. Planar interfaces have the dimension 2 ($D = 2$), while the tip of a moving needle domain is a line in three dimensions and represents the case $D = 1$. Boundaries well beyond the depinning threshold move freely as solitary waves; their behavior has been well described in the literature [63].

In Fig. 1.12, the trajectory of a needle domain in $LaAlO_3$ is shown. The advancing or retracting needle domain is pinned by defects that are mostly located

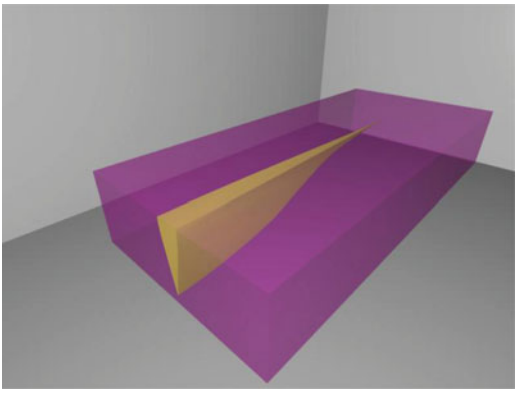

Fig. 1.12 Shape of a needle domain inside the ferroelastic matrix. The advancing front ($D = 1$) is pinned by a small number of defects

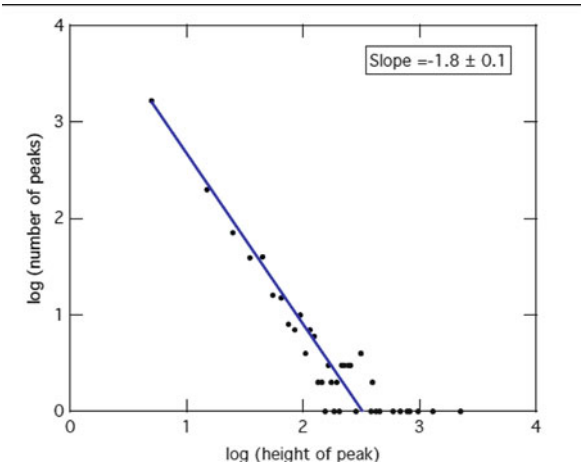

Fig. 1.13 Power law dependence of the energy emission of a single advancing needle domain ($D = 1$). The exponent is estimated to be ~ -1.8

at the advancing edge of the hull-shaped domain. Pinning is then described as the local fixation of a line in three-dimensional space, $D = 1, d = 3$. It is not trivial that pinning should occur at all in this scenario: the Larkin length of the edge in elastic systems is assumed to be large and very strong pinning centers are required in order to obtain the pinning of the advancing needle (Fig. 1.13).

In this context, the recent contribution of Proville [64] is relevant. He showed that in cases where the Larkin length is larger than the system size one can still expect avalanches with a finite depinning force. This observation calls into question the traditional way how the Larkin length is simulated in computer experiments: the elasticity of the interface is simply represented by interatomic springs between

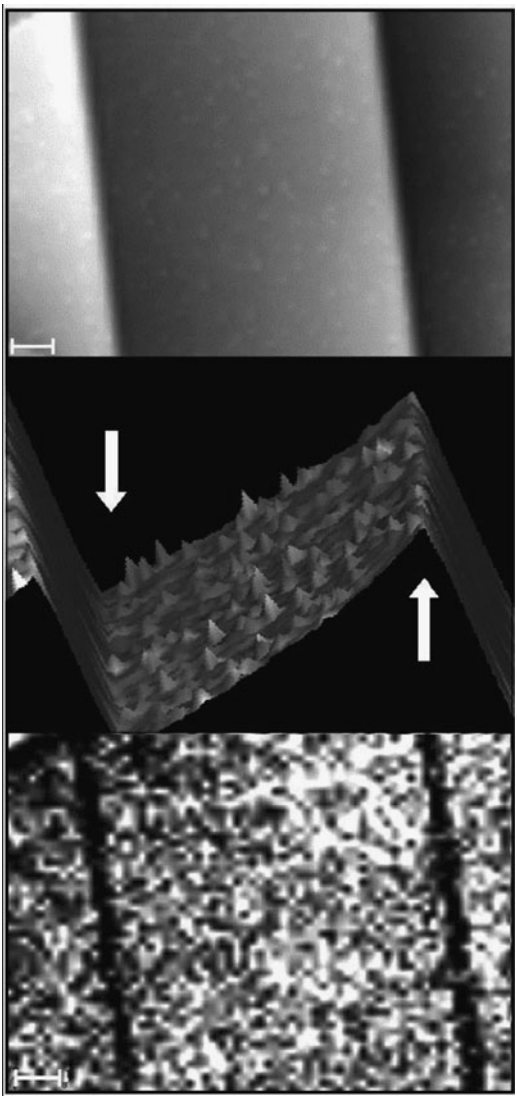

Fig. 1.14 Optical (*top*) and AFM images of twin boundaries in $Pb_3(PO_4)_2$ with high number of Ba defects (courtesy U. Bismayer, University of Hamburg) [33,34]. Scale bar is 6 μm. The pinning by Ba is very weak indicating that the Larkin length is very long

atoms in the wall. This is not the sole obvious mechanism in ferroelastic systems, however. It was shown [65] that the two major forces acting on the interface – in addition to the wall energy itself – are the "anisotropy energy" (which is minimal for walls with an orientation where the compatibility relation is satisfied). Any rotation of a wall segment requires significant energy $\sim \cos\varphi$ (in a local approximation), where φ is the angle between the stress-free equilibrium direction and the actual

direction of the wall segment. The second important energy is the wall "bending energy," which resists any curvature of the wall and is particularly large in case of thick walls [65]. These energies will act against the roughening of walls and ensures that twin walls remain globally planar even under doping conditions, which would normally lead to rough walls in magnetic systems. Such walls would meander in order to take advantage of as many defects as feasible to obtain a maximum pinning force. The AFM image in Fig. 1.9 shows the case of Ba-doped $Pb_3(PO_4)_2$ where no significant pinning is achieved by the addition of the Ba atoms. The moving wall does not meander and remains smooth. It can wrap around defects whenever they encounter such defects or defect clusters. The characteristic length is then given by the geometry of the defect and the details of the elastic interactions and is much longer than the classic Larkin length. This leads to the question: how individual defects contribute to the wall pinning. It is no wonder, therefore, that a simple "elastic" model which leads to the formulation of the Larkin length cannot – in most realistic cases – correctly describe the pinning behavior in martensitic, ferroelastic, and other ferroic domain structures (Fig. 1.14).

1.5 Conclusions

Multiferroic materials are well established. For some systems, such as $BiFeO_3$, industrial applications seem to be within our reach during the next decade. The key is a firm understanding of the coupling between the various order parameters in the bulk. The theory for the various mechanisms is also well established even in cases where the exact atomic nature of the coupling mechanism remains unclear. The open question is what new developments we can expect in the next 5 years?

The first development is to consider conductivity and even superconductivity as an equally important feature as multiferroicity. The treatment of high carrier densities and pairing mechanisms can follow the same path as the treatment of coupling between elastic, magnetic, and electric degrees of freedom.

Disruptive technologies can be envisaged if we succeed to use interfaces as active elements in multiferroic and other functional materials. This idea is new and finds its expression in the terminology of "domain boundary engineering." Theoretically, coupling between various properties in domain boundaries is easier than in the bulk: the coupling need not be related to terms such as $Q_1^2 Q_2^2$ in the relevant Hamiltonian (where Q is understood as an order parameter, which is constant over a length scale of several interatomic distances, at least). Instead, we have many more coupling phenomena at our disposal, such as the all important gradient coupling. Strong coupling such as seen in flexo-elasticity of the type $Q_1 \nabla Q_2$ and the interference of the gradient term $(\nabla Q)^2$ for each order parameter opens the door for a multitude of novel effects that contain hereto unknown structural states on a length scale of the thickness of interfaces (i.e. some nm). The same terms apply when we consider conducting interfaces that can play the role of electric wiring in devices.

References

1. E. Ascher, H. Rieder, H. Schmid, H. Stossel, Some properties of ferromagnetoelectric nickel-iodine boracite Ni3B7O13. J. Appl. Phys. **37**, 140 (1966)
2. S. Kinge, M. Crego-Calama, D.N. Reinhoudt, Self-assembling nanoparticles at surfaces and interfaces. ChemPhysChem **1**, 20 (2008)
3. M. Fiebig, Revival of the magnetoelectric effect. J. Appl. Phys. D **38**, R123 (2005)
4. J. Wang, J.B. Neaton, H. Zheng, V. Nagarajan, S.B. Ogale, B. Liu, D. Viehland, V. Vaithyanathan, D.G. Schlom, U.V. Waghmare, N.A. Spaldin, K.M. Rabe, M. Wuttig, R. Ramesh, Epitaxial BiFeO3 multiferroic thin film heterostructures. Science **299**, 1719 (2003)
5. A. Lubk, S. Gemming, N.A. Spaldin, First-principles study of ferroelectric domain walls in multiferroic bismuth ferrite. Phys. Rev. B **80**, art. 104110, (2009)
6. N.A. Spaldin, M. Fiebig, The renaissance of magnetoelectric multiferroics. Science **309**, 391 (2005)
7. J.B. Neaton, C. Ederer, U.V. Waghmare, N.A. Spaldin, K.M. Rabe, Elastic behavior associated with phase transitions in incommensurate Ba2NaNb5O15. Phys. Rev. B **71**, art. 014113 (2005)
8. E.K.H. Salje, Phase Transitions in ferroelastic and co-elastic crystals (Cambridge University Press, Cambridge, UK, 1993)
9. J.C. Lashley, S.M. Shapiro, B.L. Winn, et al., Observation of a continuous phase transition in a shape-memory alloy. Phys. Rev. Lett. **101**, art. 135703 (2008)
10. W. Eerenstein, N.D. Mathur, J.F. Scott, Multiferroic and magnetoelectric materials. Nature **442**, 759 (2006)
11. E.K.H. Salje, Multiferroic domain boundaries as active memory devices: Trajectories towards domain boundary engineering. ChemPhysChem **11**, 940 (2010)
12. S. Marais, V. Heine. C. Nex, et al., Phenomena due to strain coupling in phase – transitions. Phys. Rev. Lett. **66**, 2480 (1991)
13. M.A. Carpenter, E.K.H. Salje, Elastic anomalies in minerals due to structural phase transitions. Eur. J. Mineral. **10**, 693 (1998)
14. S.H. Lim, M. Murakami, W.L. Sarney, et al., The effects of multiphase formation on strain relaxation and magnetization in multiferroic BiFeO3 thin films. Adv. Func. Mater. **17**, 2594 (2007)
15. R.D. James, M. Wuttig, Magnetostriction of martensite. Phil Mag. A **77**, 1273 (1998)
16. K. Mori, M. Wuttig, Magnetoelectric coupling in terfenol-D/polyvinylidenedifluoride composites, Appl. Phys. Lett. **81**, 100 (2002)
17. J. Wang, J.B. Neaton, H. Zheng, et al., Epitaxial BiFeO3 multiferroic thin film heterostructures. Science **299**, 1719 (2002)
18. J. Seidel, L.W. Martin, Q. He, et al., Conduction at domain walls in oxide multiferroics. Nat. Mater. **8**, 229 (2009)
19. N. Hur, S. Park, P.A. Sharma, et al., Electric polarization reversal and memory in a multiferroic material induced by magnetic fields. Nature 429, 392 (2004)
20. C. Ederer, N.A. Spaldin, Weak ferromagnetism and magnetoelectric coupling in bismuth ferrite, Phys. Rev. B **71**, art. 060401 (2005)
21. A. Aird, E.K.H. Salje, Sheet superconductivity in twin walls: experimental evidence of WO3-x. J. Phys.: Condens. Matter **10**, L377 (1998)
22. B. Nagaraj, T. Sawhney, S. Perusse, et al., (BaSr)TiO3 thin films with conducting perovskite electrodes for dynamic random access memory applications. Appl. Phys. Lett. **74**, 3194 (1999)
23. S. Ramesh, V.P. Kumar, P. Kistaiah, et al., Preparation, characterization and thermo electrical properties of co-doped Ce0.8- xSM0.2CaxO2 (-) (delta) materials. Solid State Ionics **181**, 86 (2010)
24. T. Shimada, S. Tomoda, T. Kitamura, Ab initio study of ferroelectric closure domains in ultrathin PbTiO3 films. Phys. Rev. B **81**, art 144116 (2010)
25. S.E. Barnes, S. Maekawa, Current-spin coupling for ferromagnetic domain walls in fine wires. Phys. Rev. Lett. **95**, art. 107204 (2005)

26. E.K.H. Salje, J. Chrosch, R.C. Ewing, Is "metamictization" of zircon a phase transition? Am. Mineral. **84**, 1107 (1999)
27. S. Rios, E.K.H. Salje, M. Zhang, et al., Amorphization in zircon: evidence for direct impact damage, J. Phys.: Condens. Matter **12**, 2401 (2000)
28. S. Sarkar, X.B. Ren, K. Otsuka, Evidence for strain glass in the ferroelastic-martensitic system Ti50-xNi50+x. Phys. Rev. Lett. 95, art. 205702 (2005)
29. B. Noheda, D.E. Cox, G. Shirane, et al., Phase diagram of the ferroelectric relaxor (1-x)PbMg1/3Nb2/3O3-xPbTiO(3), Phys. Rev. B **66**, art. 054104 (2002)
30. A. Levstik, Z. Kutnjak, C. Filipic, et al., Glassy freezing in relaxor ferroelectric lead magnesium niobate. Phys. Rev. B **57**, 11204 (1998)
31. G.A. Samara, The relaxational properties of compositionally disordered ABO(3) perovskites. J. Phys.: Condens. Matter **15**, R367 (2003)
32. J. Chrosch, E.K.H. Salje, Near-surface domain structures in uniaxially stressed SrTiO3. J. Phys.: Condens. Matter **85**, 722 (1999)
33. J. Chrosch, E.K.H. Salje, Temperature dependence of the domain wall width in LaAlO3. J. Appl. Phys. **85**, 722 (1999)
34. B. Wruck, E.K.H. Salje, M. Zhang, et al., On the thickness of ferroelastic twin walls in lead phosphate Pb3(PO4)2 – an X-ray diffraction study. Phase Transit. **48**, 135 (1994)
35. E.K.H. Salje, H. Zhang, A. Planes, et al., Martensitic transformation B2-R in Ni-Ti-Fe: experimental determination of the Landau potential and quantum saturation of the order parameter. J. Phys.: Condens. Matter **20**, art. 275216 (2008)
36. E.K.H. Salje, H. Zhang, D. Schryvers, et al., Quantitative Landau potentials for the martensitic transformation in Ni-Al. Appl. Phys. Lett. **90**, art. 221903 (2007)
37. M. Calleja, M.T. Dove, E.K.H. Salje, Trapping of oxygen vacancies on twin walls of CaTiO3: a computer simulation study. J. Phys.: Condens. Matter **15**, 2301 (2003)
38. W.T. Lee, E.K.H. Salje, L. Goncalves-Ferreira, et al., Intrinsic activation energy for twin-wall motion in the ferroelastic perovskite CaTiO3. Phys. Rev. B **73**, art. 214110 (2006)
39. L. Goncalves-Ferreira, S.A.T. Redfern, E. Artacho, et al., Ferrielectric twin walls in CaTiO3. Phys. Rev. Lett. **101**, art. 097602 (2008)
40. L. Goncalves-Ferreira, S.A.T. Redfern, E. Atacho, et al., The intrinsic elasticity of twin walls: Ferrielectric twin walls in ferroelastic CaTiO3. Appl. Phys. Lett. **94**, art. 081903 (2009)
41. L. Goncalves-Ferreira, S.A.T. Redfern, E. Artacho, et al., Trapping of oxygen vacancies in the twin walls of perovskite. Phys. Rev. B **81**, art. 024109 (2010)
42. P. Zubko, G. Catalan, P.R.L. Welche, A. Buckley, J.F. Scott, Strain-gradient-induced polarization in SrTiO3 single crystals. Phys. Rev. Lett. **99**, art.167601 (2007)
43. A.K. Tagantsev, E. Courtens, L. Arzel, Prediction of a low-temperature ferroelectric instability in antiphase domain boundaries of strontium titanate. Phys. Rev. B **64**, art.224107 (2001)
44. J. Petzelt, T. Ostapchuk, I. Gregora, I. Rychetsky, S. Hoffmann-Eifert, A.V. Pronin, Y. Yuzyuk, B.P. Gorshunov, S. Kamba, V. Bovtun, J. Pokorny, M. Savinov, V. Porokhonskyy, D. Rafaja, P. Vanek, A. Almeida, M.R. Chaves, A.A. Volkov, M. Dressel, R. Waser, Dielectric, infrared, and Raman response of undoped SrTiO3 ceramics: Evidence of polar grain boundaries. Phys. Rev. B **64**, art.184111 (2001)
45. W. Zhong, D. Vanderbilt, Competing structural instabilities in cubic perovskites. Phys. Rev. Lett.**74**, art. 2587 (1995)
46. E.K.H. Salje, A pre-martensitic elastic anomaly in nanomaterials: elasticity of surface and interface layers. J. phys.: Condens. Matter **20**, art. 485003 (2008)
47. A. Aird, E.K.H. Salje, Enhanced reactivity of domain walls in WO3 with sodium. Eur. Phys. J. B **15**, 205 (2000)
48. A. Aird, M.C. Domeneghetti, F. Mazzi, et al., Sheet superconductivity in WO3-x: crystal structure of the tetragonal matrix, J. Phys.: Condens. Matter **10**, L569 (1998)
49. R.A. de Groot, F.M. Mueller, P.G. van Engen, K.H.J. Buschow, New class of materials: Half-metallic ferromagnets. Phys. Rev. Lett. **50**, 2024 (1983)

50. E.K.H. Salje, S. Rehmann, F. Pobell, D. Morris, K.S. Knight, T. Herrmanndörfer, M.T Dove, Crystal structure and paramagnetic behaviour of epsilon-WO3-x. J. Phys.: Condens. Matter **9**, 6563 (1997)
51. E. Salje, A.F. Carley, M.W. Roberts, Effect of reduction and temperature on the electronic core levels of tungsten and molybdenum in WO3 and WxMo1-xO3 – photoelectron spectroscopy study. J. Solid State Chem. **29**, 237 (1979)
52. F.H. Jones, K. Rawlings, J.S. Foord, R.G. Egdell, J.B. Pethica, B.M.R. Wanklyn, S.C. Parker, P.M. Olive, An STM study of surface structures on WO3(001). Surf. Sci. **359**, 107 (1996)
53. O.F. Schirmer, E. Salje, Conduction bipolarons in low-temperature crystalline WO3-x. J. Phys.: Condens. Matter **13**, 1067 (1980)
54. O.F. Schirmer, E. Salje, W5+ polaron in crystalline low-temperature WO3 electron spin resonance and optical absorption. Solid State Comm. **33**, 333 (1980)
55. S. Reich, G. Leitus, R. Popovitz-Biro, A. Goldbourt, S. Vega, A possible 2D H (x) WO3 superconductor with a T (c) of 120 K. J. Supercond. Novel Magnetism **22**, 343 (2009) and reference given there
56. Y. Kim, M. Alexe, E.K.H. Salje, Nanoscale properties of thin twin walls and surface layers in piezoelectric WO3-x. Appl. Phys. Lett. **96**, art. 032904 (2010)
57. E. Vives, J. Ortin, L. Manosa, et al., Distribution of avalanches in martensitic transformations. Phys. Rev. Lett. **72**, 1694 (1994)
58. E. Bonnot, E. Vives, L. Mañosa, et al., Acoustic emission and energy dissipation during front propagation in a stress-driven martensitic transition. Phys. Rev. B **78**, art. 094104 (2008)
59. M.C. Kuntz, J.P. Sethna, Noise in disordered systems: The power spectrum and dynamic exponents in avalanche model. Phys. Rev. B **62**, art. 11699 (2000)
60. M.C. Gallardo, J. Manchado, F.J. Romero, et al., Avalanche criticality in the martensitic transition of Cu67.64Zn16.71Al15.65 shape-memory alloy: A calorimetric and acoustic emission study. Phys. Rev. B **81**, art.174102 (2010)
61. E.K.H. Salje, L. Koppensteiner, M. Reinecker, et al., Jerky elasticity: Avalanches and the martensitic transition in Cu74.08Al23.13Be2.79 shape-memory alloy. Appl. Phys. Lett. **95**, art. 231908 (2009)
62. A. Rosso, P. Le Doussal, K.J. Wiese, Avalanche-size distribution at the depinning transition: A numerical test of the theory. Phys. Rev. B **80**, art. 144204 (2009)
63. M.C. Kuntz, O. Perkovic, K.A. Dahmen, et al., Hysteresis, avalanches, and noise. Comput. Sci. Eng. **1**, 73 (1999)
64. L. Proville, Depinning of a discrete elastic string from a random array of weak pinning points with finite dimensions. J. Stat. Phys. **137**, 717 (2009)
65. E.K.H. Salje, Y. Ishibashi, Mesoscopic structures in ferroelastic crystals: Needle twins and right-angled domains. J. Phys.: Condens. Matter **8**, 8477 (1996)

http://www.springer.com/978-3-642-20942-0

Disorder and Strain-Induced Complexity in Functional Materials

Kakeshita, T.; Fukuda, T.; Saxena, A.B.; Planes, A. (Eds.)
2012, XVI, 308 p., Hardcover
ISBN: 978-3-642-20942-0